

Research Article

Gabriel Ertz*, Jens Twiefel and Malte Krack

Feasibility Study for Small Scaling Flywheel-Energy-Storage Systems in Energy Harvesting Systems

Abstract: Two concepts of scaled micro-flywheel-energy-storage systems (FESSs): a flat disk-shaped and a thin ring-shaped (outer diameter equal to height) flywheel rotors were examined in this study, focusing on material selection, energy content, losses due to air friction and motor loss. For the disk-shape micro-FESS, isotropic materials like titanium, aluminum, steel and wolfram are shown to be suitable as a flywheel rotor. Wound fiber reinforced composite plastics (T1000-, T300-carbon fibers and carbon nanotubes “CNTs”) were investigated for the flywheel in a ring shape. It was shown that isotropic materials reach the highest energy densities in the shape of a Laval disk with a rim. A micro-FESS with wolfram flywheel would reach the highest half-time-periods due to its high density, and thus, it is the favored material to design a flat disk-shaped micro-FESS with low standby-losses. Fiber reinforced plastic flywheels in ring shape reach the highest energy densities, from 150 W h/kg (T300) to 2,600 W h/kg (CNT), but display higher standby-losses as well. A scaling of the rotors was done within this study and showed that air friction is influenced by the shape of the examined flywheel rotors and the material. A linear correlation of down scaling and air friction losses was shown. As a motor/generator type, an ironless air coil Halbach array motor was suggested. Motor losses due to eddy currents in the stator coil were estimated. Losses correlated in square with downscaling. FESSs with wolfram and CNT showed the lowest standby-losses due to eddy currents.

Keywords: micro-FESS, flywheel, micro energy storage, energy harvester

DOI 10.1515/ehs-2013-0010

*Corresponding author: **Gabriel Ertz**, Institute of Dynamics and Vibration Research (IDS), Appelstraße 11, D-30167 Hannover, Germany, E-mail: g-ertz@web.de

Jens Twiefel: E-mail: twiefel@ids.uni-hannover.de, **Malte Krack:** E-mail: krack@ids.uni-hannover.de, Institute of Dynamics and Vibration Research (IDS), Appelstraße 11, D-30167 Hannover, Germany

Introduction

Flywheel-energy-storage systems (FESSs) are finding an increasing number of practical applications. There are several instances where they were used for short-time energy storage, e.g. Kinetic Energy Recovery System known as “KERS” in Formula 1 cars, within the metro system “Üstra” in Hanover, or for uninterruptable power supply in computer-systems in cases of emergency. Micro-FESSs that are applicable in energy harvester systems, with a diameter of 35 mm, have been realized in Yoo (2008 in COEX). Due to the downscaling of manufacturing methods, FESSs could be realized to an even smaller dimension. Presently, high specific strength materials, e.g. high tensile stress carbon fibers as “T1000”, increased the energy density of flywheels to 100 W h/kg (including housing). Due to its enormously high specific yield strength, prospective materials like carbon nanotubes (CNTs) could increase the energy density to about 2,500 W h/kg (without housing, 900 W h/kg including housing) and thus compete with a new generation of “(nanoporous carbon) electric double-layer supercapacitors” (EDLC) that have been developed as a prototype with an energy density of 300 W h/kg (without housing) (Hu 2007). Chemical batteries (Zinc-Air-Battery) have reached an energy density of 450 W h/kg, although they are not rechargeable. Available efficient rechargeable batteries, as Lithium-Ion-Batteries, reach an energy density of up to 200 W h/kg. Furthermore, contactless electro-dynamic bearings for flywheels have been developed (Bleuler and Sandtner 2005) that operate at high rotational velocity and replace roller bearings to reduce bearing friction and extend the FESS lifetime. In comparison to chemical batteries, FESSs have a great advantage concerning lifecycles, efficiency, discharging and charging times and power density. Figure 1 shows the power density vs energy density of different storage devices.

A future application of FESS might be the power supply of sensor actor networks in trains and especially in

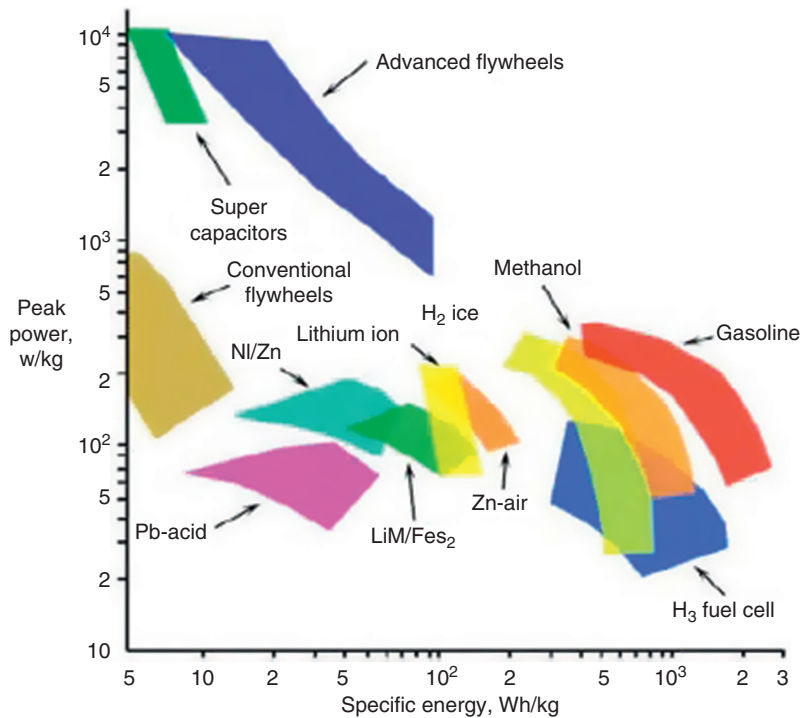


Figure 1 Ragone chart of existing power sources (Ghoniem 2011)

airplanes. The Airbus Group and a researchers group of turbine manufacture Rolls Royce are looking for a new energy source to supply the many sensors in airplanes, specifically in the turbine, since the wires that are used to connect the sensors to the power source, the weight and the volume of the wires were problematic. Instead, energy harvesters could be used to supply wireless sensors. For a constant power supply from these sensors, a battery is required in situations when the harvester cannot provide enough power. A lifespan of more than 30 years and a high reliability of the harvester-battery-system have the highest priorities. Since FESSs achieve lifetimes of decades and reach the energy density of Li-ion batteries and a similar power density as super capacitors, they would be very suitable for this application. In this study, the downscaling feasibility of FESSs for Energy Harvesting (EH) applications is investigated. A loss calculation was done to estimate the half-time of small-scaled FESS. Two designs are investigated and scaled in size: a flat disk-shaped FESS and a cylindrical FESS. Besides the shape, different materials like aluminum, titanium, steel, wolfram and three types of carbon fiber reinforced plastics (CFRPs) with T1000 and T300 carbon fibers as well as CNTs have been studied. The following sections give an overview of the loss calculation, the effect of scaling and the assumptions that were applied.

FESS physical relations

There are two types of FESS rotors that can be taken into account for a high specific energy density: a flat disk rotor out of isotropic material (shape 1) and a cylindrical design with fiber reinforced plastics with fibers oriented in circumferential direction (orthotropic) (shape 2).

Shape 1: Laval-disk-with-rim

The equation to determine the energy content E_{kin} of a flywheel for a solid disk is

$$E_{\text{kin}} = \frac{1}{2} * J * \omega^2 \quad [1]$$

with

$$J = \frac{1}{2} * m * r^2 \quad [2]$$

where m represents the mass of the flywheel, r the radius and ω the angular velocity.

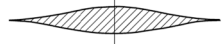

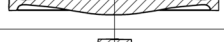

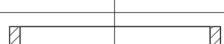

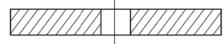

For isotropic materials, the energy density is limited by the maximum radial strength in the rotor and directly

influences the energy density (energy-to-mass-ratio $\frac{E}{m}$) that can be written as:

$$\frac{E}{m} = K * \frac{\sigma_{\max}}{\rho}. \quad [3]$$

with shape factor K and maximum stress σ_{\max} . Table 1 shows different shapes with the corresponding shape factors. A shape factor of $K = 1$ for a Laval disk is practically not achievable since it considers an infinitely thin fringe at the radius with value infinity. Hence a bigger rim at the outer radius of the Laval disk replaces the infinite thin fringe and allows a shape factor of $K = 0.95$. This shape combines a high energy density and high energy content due to the increasing momentum of inertia caused by the rim. For the further stress calculation *shape 1* is assumed to be a Laval-disk-with-rim with a shape factor of $K = 0.95$ (Table 1).

Table 1 Shape factor K of possible flywheel shapes

Laval disk		1.00
Laval disk real		0.70–0.90
Laval-disk-with-rim		0.8–0.95
Conical disk		0.70–0.85
Solid disk		0.606
Thin ring		0.50
Disk with rim and centerhole		0.40–0.50
Thick rim		0.303

Shape 2: thin ring

Thin rings, constructed out of orthotropic materials like fiber composites, show two specific properties in comparison to disk-shaped isotropic materials:

1. The maximum stress occurs in circumferential direction, which is in the fiber direction of the composite materials. Since carbon fibers show an enormous strength in the fiber direction, they are an optimal material to take the circumferential stress. Due to the slender ring thickness, radial stress that normally limits the flywheel performance and that would be taken mostly by the resin is negligible.
2. The momentum of inertia grows differently (see eq. [4]) in comparison to the mass (see eq. [5]) concerning the radii ratio r_i/r_a

$$J = \frac{1}{2} * \rho * V * (r_i^2 + r_a^2) = \frac{1}{2} * \rho * \underbrace{\pi * (r_a^2 - r_i^2) * h}_{\substack{V \\ m}} * (r_i^2 + r_a^2) \quad [4]$$

$$m = \rho * \pi * (r_a^2 - r_i^2) * h \quad [5]$$

so that a high radii ratio causes an increasing energy density as can be seen in Figure 2

If CNTs can be produced in length of cm instead of mm they would be suitable for FESS and could increase energy density of a FESS up to 2,900 W h/kg since they reach a yield strength of around 30 GPa (Yu 2000). For

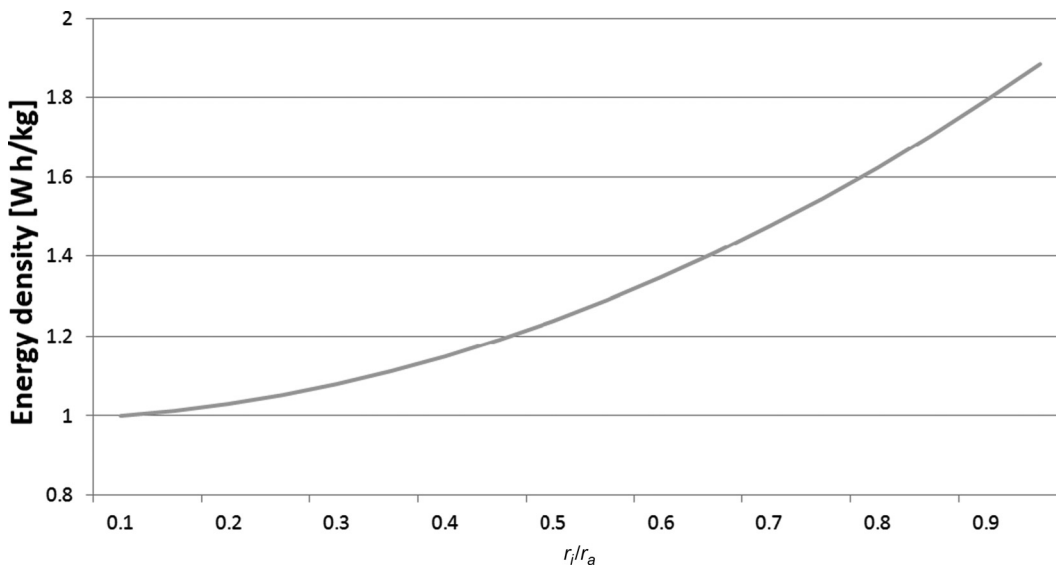


Figure 2 Energy density depending on radii ratio r_i/r_a

further calculations of *shape 2*, a radii ratio r_i/r_a of 0.9 was set. That allows us to use a simple equation for calculating the limiting circumferential stress for thin rims (Feldhusen 2001):

$$\sigma_\theta \approx \rho * r^2 * \omega^2. \quad [6]$$

For thin rims, with a radii ratio r_i/r_a of 0.9, the shape factor decreases to $K = 0.45$ and thus the energy density is calculated according to

$$\frac{E}{m} \approx \frac{r^2 * \omega^2}{2.2} \approx K * \frac{\sigma_{\max}}{\rho}. \quad [7]$$

Scaling of two flywheel concepts

To see how downscaling affects the energy content, the rotational velocity and the losses due to gas and motor friction, two concepts with the following dimensions relations are considered:

Ring:	Disk:
$d_2 = 1.5 - 30\text{mm}$	$V_{\text{ring}} = V_{\text{disc}}; m_{\text{ring}} = m_{\text{disc}}$
$h_{\text{ring}} = d_2$	$R_0 = \sqrt[3]{10h_{\text{ring}}(r_a^2 - r_i^2)}$
$d_1 = 0.9 * d_2$	$D_0 = 1.9 - 37\text{mm}$
Vacuum in both cases: $1*10^{-4}$ mbar	$H_{\text{disc}} = 0.1R_0$

The CFRP-ring and the Laval-disk-with-rim shapes can be seen in Figure 3 where the Laval-disk-with-rim is assumed to be a disk with the same momentum of inertia and volume to allow the use of a less complex air loss estimation. Whenever disk shape is mentioned in the following, they imply the properties of the Laval-disk-with-rim.

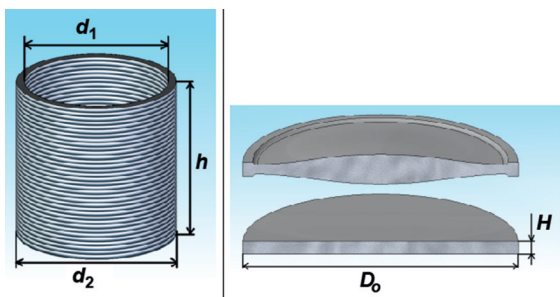


Figure 3 Schematic shape 1: ring (left), shape 2: Laval-disk-with-rim (top right) and a solid disk (bottom right) used for the simplified air loss estimation

Table 2 Energy densities of different flywheel materials at disk and ring shape (Torayca, T1000 Data Sheet; Torayca, T300 Data Sheet)

Material	Yield strength [MPa]	Density ρ [kg/m ³]	Energy density $\frac{E}{m}$ [W h/kg] ring $r_i/r_a = 0.9$	Laval-disk-with-rim $K = 0.95$
CNT	30,000	1,400	2,693	–
T1000	3,040	1,500	254	–
T300	1,860	1,500	156	–
Resin (for comparison)	69	1,151	7.6	16
Titanium TiAl6V4	1,100	4,430	32.3	65.5
Steel 60SiCr7	1,400	7,430	24.5	49.7
Aluminum AW-7075	400	2,700	19.3	39.1
Wolfram	1,920	19,300	12.9	26.3

The mass specific energy densities are shown in Table 2. They are calculated after eqs [3] and [7] and take into account the maximum feasible rotational velocity that is limited by the yield strength. Furthermore, the mass specific energy densities are independent of the absolute dimensions. As can be seen, the energy density of the isotropic material is highest at the disk shape due to the increase of the shape factor K . The orthotropic materials show higher absolute energy densities since the strain-to-density ratio is higher. Energy densities for composite materials in disk shapes are not examined. In this case, the radial stress would be the limiting factor, which would only be determined by the comparatively low strength of the resin.

Figure 4 shows the maximum resulting rotational velocity $n = \frac{\omega * 60}{2 * \pi}$ for the given yield strength of the different flywheel materials at the different shapes. Since the CFRPs are light and show high yield strength values, the rotational velocity of them is generally higher than that of metal flywheels. Due to the better stress distribution the metals show higher speed in a disk shape than in a ring shape.

With eq. [1], the absolute energy content of the flywheel geometries is calculated for a maximum achievable rotational velocity (see Figure 5). The highest energy content can be achieved with CNTs in a ring shape. Since the volume between ring and disk shapes is equal, the CNTs also show the best energy content-to-volume ratio. Wolfram shows the second highest energy content but only in a disk shape. Steel, in a disk shape and the T1000 composite ring, shows equivalent energy contents. The least favorable materials are titanium and aluminum when it comes to energy density regarding the volume since these materials are too light to reach adequate values.

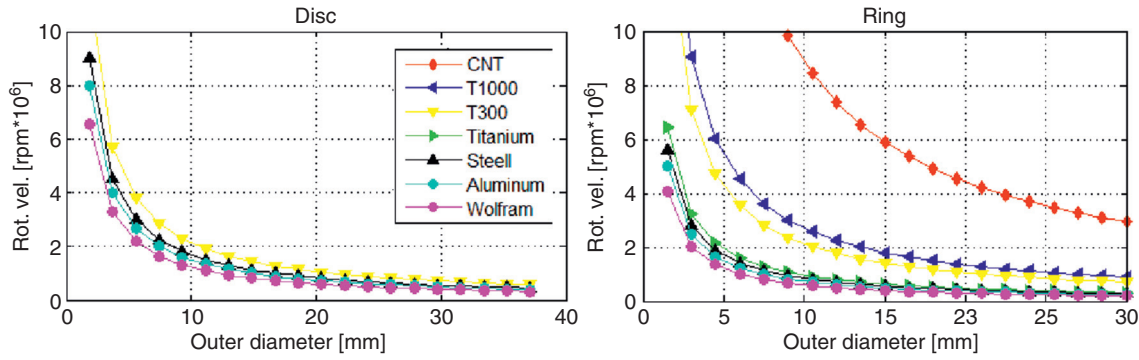


Figure 4 Maximum rotational speed vs. diameter for disk (left) and ring (right)

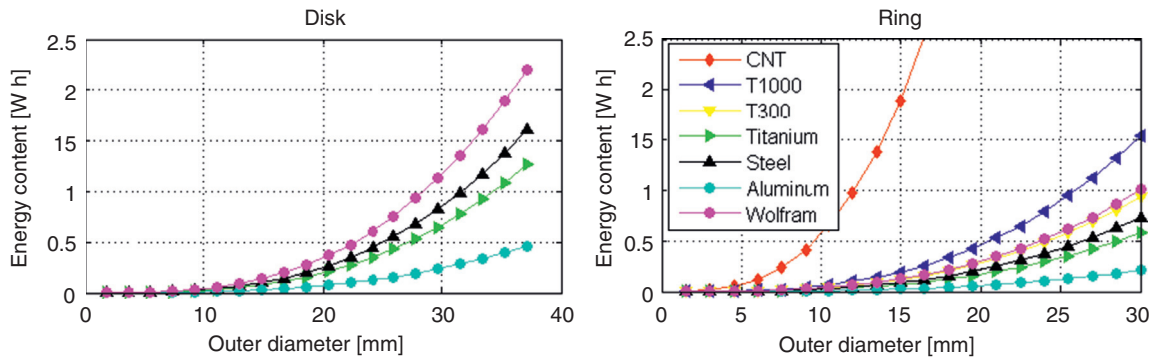


Figure 5 Energy content vs. diameter for disk shape (left) and ring shape (right)

Air friction

Smaller flywheels have a smaller ratio between mass (correlated to stored energy) and surface (correlated to gas friction), and hence, the gas friction which is proportional to the surface increases. The gas friction (P_{gas}) can be calculated (Kolk 1997) assuming molecule to housing impacts only and no molecule to molecule impacts that would cause a viscous fluid. Since a micro-FESS would run in a highly evacuated vacuum with a rest pressure of less than $1 \cdot 10^{-4}$ mbar, the assumption of molecule to housing impacts would be valid up to a flywheel to housing distance of 1 m.

When a molecule hits the spinning rotor it transfers its momentum:

$$\Delta \bar{L} = m_m \omega r^2 \text{ with molecule mass } m_m \quad [8]$$

at an average

$$z = \frac{n_m}{4} \bar{c} \quad [9]$$

molecule per time unit hits a specific rotor surface, where

$$n_m = \frac{N}{V} = \frac{p_G}{k_B T} \quad [10]$$

is equal to the density of molecules at pressure p_G . \bar{c} is the average molecule velocity is governed by the Maxwell equation:

$$\bar{c} = \sqrt{\frac{8k_B T}{\pi m_m}}. \quad [11]$$

Thus, the transferred angular momentum of inertia due to molecule impacts is

$$\begin{aligned} \bar{L} &= T_G = z m_m \omega \int r^2 dA \\ &= \sqrt{\frac{1}{2\pi}} \sqrt{\frac{m_m}{k_B T}} p_G \omega \int r^2 dA. \end{aligned} \quad [12]$$

This leads to the total gas friction losses with the rotational velocity equal to

$$P_{\text{Gas}} = T_G \omega \quad [13]$$

with an area of circle given as

$$\int_{\text{disc}} r^2 dA = \int_0^{r_a} \int_0^{2\pi} r^2 r d\varphi dr = \frac{\pi}{2} r_o^4 \quad [14]$$

and the lateral area

$$\int_{\text{lateral}} r^2 dA = \int_0^h \int_0^{2\pi} r^2 r d\varphi dh = 2\pi h r_o^3. \quad [15]$$

The gas friction losses P_{Gas} for a solid disk is thus

$$P_{\text{Gas,disc}} = \sqrt{\frac{\pi M}{2 R_G T}} p_G \omega^2 r_o^3 (r_o + 2h) \quad [16]$$

and for a thin ring

$$P_{\text{Gas,ring}} = \sqrt{\frac{\pi M}{2 R_G T}} p_G \omega^2 2h (r_1^3 + r_2^3) \quad [17]$$

with $M = N_A m_m$ and $R_G = N_A k_B = 83,145 \frac{\text{J}}{\text{molK}}$.

M : molar mass

R_G : molar gas constant

T : temperature

p : pressure

h : flywheel height

N_A : Avogadro constant

Figure 6 shows the half-time-period τ_{gas} due to gas friction, P_{Gas} , that can be calculated as

$$\tau_{\text{gas}} = \ln(2) * \frac{E_{\text{kin}}}{P_{\text{Gas}}} \quad [18]$$

and demonstrates the time period for the rotor to lose half of its kinetic energy content. Flywheels of disk shapes show 1.8 times longer half-time-periods than ring shapes, due to their larger surfaces. The air friction has also high effects on materials with lower density since they spin faster. Air friction increases proportional to the fourth degree of the flywheel radius $P_{\text{Gas}} \sim r^4$, the energy content increases proportional to the fifth degree $E_{\text{kin}} \sim r^5$. Hence, the half-time-period increases linearly with a bigger rotor radius. The rotational velocity has no influence on τ_{gas} , since both P_{Gas} and E_{kin} increase quadratically with the velocity. The density has a specific value for each material and only influences the energy content. For this reason, the half-time-period τ_{gas}

for heavy materials increases by a factor of the density relation. Thus, τ_{gas} for wolfram rotors is 2.6 times higher than τ_{gas} for steel rotors due to $\frac{\rho_{\text{wolfram}}}{\rho_{\text{steel}}} = 2.6$.

Motor/generator types for micro-FESS

Although there are plenty of different motor/generator types used in FESS applications, only a few can be considered as feasible and efficient for micro-FESSs'. A separately excited motor/generator is unfeasible since a separate power source for the excitation would be required.

Hence, permanent magnet excited motor/generator concepts would be suitable as they do not need an external power supply and can easily be controlled with a drive unit. This motor type normally contains iron in the stator winding to lead the magnetic flux toward the permanent magnets and thus increase the efficiency. Nevertheless, it is problematic that the iron causes hysteric losses at high speeds and thereby decreases the efficiency of the micro-FESS. Studies have shown that ironless air coil stators in combination with a magnetic Halbach array can reach higher efficiencies because the assembly of the magnet concentrates the magnetic field into one direction with only two magnet poles (see Figure 7). Thus, no iron core is needed to lead the magnetic flux through the stator coil.

Air coil motors are free from hysteresis iron losses but eddy current losses occur in the copper windings. The eddy currents are mainly related to the rotational velocity, the mass of the copper winding and the diameter of the copper wire. In Merritt and Post (1994), it was shown that a two-pole Halbach array air coil motor/generator (Halbach array length: 18 cm, Halbach array inner diameter: 7 cm and Halbach array outer diameter: 10.5 cm) reaches a discharging efficiency of more than 98% for a 23 kW motor made of a 1,700 strand wire bundle with 800 μm wires. A smaller

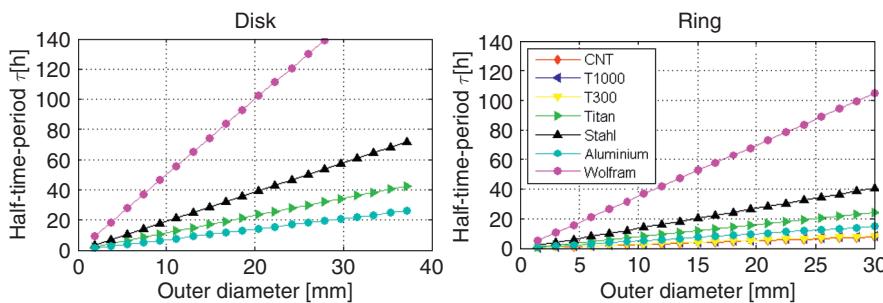


Figure 6 Half-time-period in presence of air friction vs. diameter for disk shape (left) and ring shape (right)

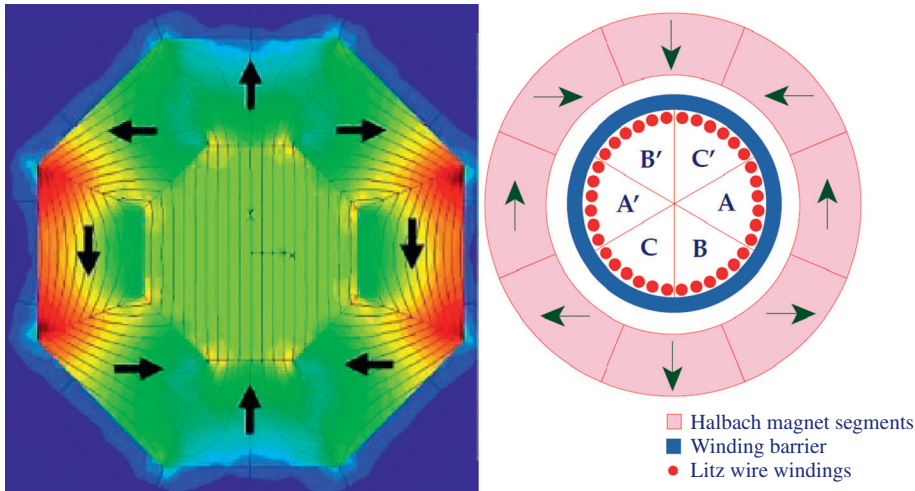


Figure 7 Magnetic flux in a Halbach array (left) and air coil motor with Halbach array scheme (right) (Merritt and Post 1994)

50 W design (2.6 cm inner stator diameter, 4.5 cm outer Halbach array diameter and 6 cm length) with four poles and a rotational velocity of up to 80,000 rpm shows an efficiency of 97% and a power density of 235 W/kg (Abdi, Milimonfared, and Moghani 2010). Also a disk motor that uses air pools and a Halbach array with 5.15 kW max. power reaches 95% efficiency and a power density of 8,100 W/kg (LaunchPoint Technologies Inc., 2009). In comparison to that, micro-motors ($d_a = 10$ mm; $h = 16$ mm) that use a conventional magnet design with several magnet poles but using an air spool show efficiencies about 69% and a power density of 91 W/kg (Faulhaber, 2013).

As demonstrated in Kratt (2010), insulated gold wires of 25 μ m diameter are manufacturable for the use of stator coils and have been wound as spools with diameter of less than 1 mm. This wire could be used to build an air spool that is located inside the ring rotor with *shape 2*. A stator for the flat *shape 1* (Laval-rotor-with-rim) is assumed to have a similar structure as tested in Yi and Lee (2007). This Korean research group developed a flat micro-motor with a sputtered gold spool as stator (Yi and Lee 2007). Their spool was made of five windings of 50 μ m high and 100 μ m thick gold conductor. The magnetic field was generated by an array of flat disk-shaped permanent magnets that were fixed onto the flywheel disk (shape: solid disk made out of high-strength aluminum). This motor with its four pole pairs accelerated a 63.2 g flywheel to a speed of 52,000 rpm at a voltage of 12 V and a power of 8 W. The energy stored in this micro-FESS was 337 J (93.6 mW h).

To increase the efficiency and the power density of the motor further, the magnets should to be magnetized in a Halbach array and should be as small as possible. For very high frequencies, as necessary for composite materials in

ring shapes, also hysteresis and eddy current losses in the magnets start playing a significant role concerning the losses. The smaller the magnets are, the lesser are the losses. Tarrant (1993) patented a method to implement magnetic material particles into the composite material and magnetize the field in a Halbach form. Thus rotor losses are negligible, and the problem of small-scaled magnets is solved. Also the magnet powder is part of the rotor and increases the momentum of inertia without having a negative effect on the composite yield strength. Hence for the motor loss calculation, only the eddy current losses that occur in the air spool are simulated.

Motor losses

An estimation of the motor losses P_{eddy} in regard to eq. [19] (Wrede 1998) was done in the following.

A gold wire was chosen as the conductor. A Halbach array with $a = 2$ magnet poles was assumed to have a magnetic flux density $\hat{B} = 0.3$ T. The flux density at the surface of a neodymium magnet is about 0.3 T. The magnetic flux in the coil would be a bit less, but this value is taken into account for a conservative calculation. The volume of the coil is hard to calculate since it depends on too many parameters like torque, maximum voltage, time to accelerate the flywheel, power and rotational velocity of the flywheel. Therefore a general ratio of coil volume to flywheel volume of $V_{\text{airspool}}/V_{\text{rotor}} = 1/1,000$ was taken from the actual design from Yi and Lee (2007) that was described before.

Due to the aluminum construction of the rotor used in the study of Yi and Lee (2007), the maximum rotational

velocity for an aluminum rotor was set as 1. To keep the voltage constant, the number of windings of the coils reduces with increasing rotational velocities. Hence, flywheels with higher rotational speeds need less gold mass to operate, due to the lesser number of windings. This is why the correction factor c_1 equals the ratio between the maximum rotational velocity of the aluminum rotor and the maximum velocity of the other design materials. The power output and thus the losses of the motor used in the ring and the Laval disk shapes are assumed to be equal at their highest reachable rotational velocity. This is taken into account by the correction factor of c_2 . This means that the gold mass for the stator spool of the ring shape is generally assumed to be less than for Laval disk shapes.

$$P_{\text{eddy}} = \frac{1}{24} * \kappa * \omega^2 * a * b^2 * \hat{B}^2 * V. \quad [19]$$

The following parameters were set based on the design proposed in Yoo (2008 in COEX):

$k = 44 * 10^6 \text{ S/m}$ electrical conductivity for gold

ω_{max} angular velocity; depend on the flywheel material and the flywheel size

$a = 2$: magnet poles for a Halbach array

$b = 25 \mu\text{m}$: wire diameter

$\hat{B} = 0.3\text{T}$: magnetic flux density

$V = \frac{1}{1,000} V_{\text{rotor,disc}} * c_1$ and $V = \frac{1}{1000} V_{\text{rotor,disc}} * c_1 * c_2$

With $c_1 = \frac{n_{\text{Aluminum}}}{n_{\text{designmaterial}}}$ and $c_2 = \frac{I_{\text{ring}}}{I_{\text{disc}}} = 1.18$

Table 3 shows the values that were calculated as a correction factor for the different flywheel materials.

Table 3 Correction factor c_1

Wolfram:	1.22
Aluminum:	1
Stahl:	0.887
Titan:	0.77
T300:	0.54
T1000:	0.42
CNT:	0.13

As can be seen in Figure 8, the half-time-period due to eddy current losses τ_{eddy} increases quadratically with bigger flywheel dimensions due to the radius relation $P_{\text{eddy}} \sim r^3$ and $E_{\text{kin}} \sim r^5$. Thus, the minimum size of the flywheel depends on the required half-time-period of the battery. Wolfram and CNT show the longest half-time-period τ_{eddy} . Aluminum can be considered as the least favorable material when it comes to motor losses.

Bearings

Depending on the size, the speed and the field of operation of the micro-FESS, different bearing types can be considered. Active magnetic bearings combined with permanent magnets can support a flywheel rotor in a moving environment with shocks and vibrations, as demonstrated in Yi and Lee (2007). This bearing type does not cause any friction but needs an external power supply and a controller unit to operate. This would be problematic with wireless sensor actor networks.

Passive bearings, such as electro-dynamic bearings, can also be used, as introduced in Sandtner and Bleuler (2004), to avoid an external controller and power unit. These magnetic bearings, using magnets rotating between copper wire coils, generate eddy currents at a certain rotational velocity. Thus, a reactive magnetic force lifts and stabilizes the flywheel without any additional controlling device. Losses are only generated when the rotor is displaced, in case of external shocks or vibrations. In combination with permanent magnets, an efficient, long-living and high-speed micro-FESS could be installed in applications with few vibrations and shocks. An illustration where a 1.3 kg rotor levitates at frequencies from 4,800 rpm onward, with 0.8 W lifting power, is given in Sandtner and Bleuler (2004). Since the electro-dynamic bearing starts working at a certain speed, touch-down bearings that only operate on low speeds, like

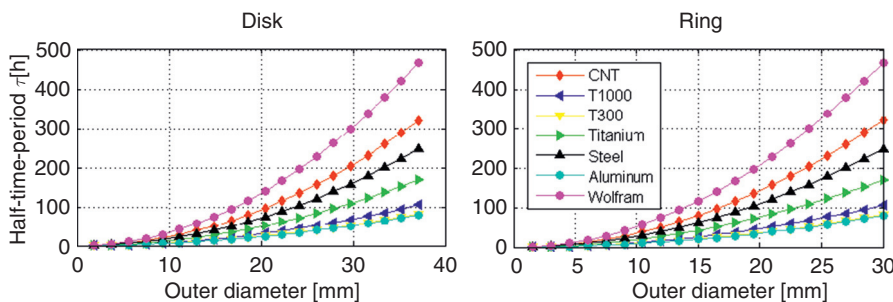


Figure 8 Half-time-period in presence of eddy current losses vs. diameter for disk shape (left) and ring shape (right)

ceramic roller bearings or jewel bearings, can be operationalized. For speeds up to 500,000 rpm, miniature ceramic roller bearings can be applied to support the rotor in environments with vibration and shocks.

Due to the variety of bearings and the different environment influences on the bearing efficiency, no bearing loss calculation was estimated. However, it can be said that roller bearings would be efficient for low-speed micro-FESS with high-density materials since friction increases linearly in relation to the speed, given by $P_{\text{roller bearing}} \sim \omega$. The higher the speed and the lower the material density, the more efficient are the electrodynamic bearings since they just generate power due to the lift force once and at rotor displacements.

Conclusions

Two types of flywheel shapes for micro-FESSs have been simulated keeping in mind the energy density, material selection, energy content, air friction and motor losses of a brushless air coil motor/generator with thin Litz wires. It was shown that isotropic materials like metals are suitable for flat disk, Laval shape with outer rim. Due to a high density, wolfram shows the best results when it comes to minimal standby-losses and high energy content-to-volume ratio. Among the examined metals, titanium shows the best mass related energy density ratio. CFRPs reach high weight specific energy densities since an optimal ring design can be selected. Energy densities 2–3 times higher than titanium can be achieved with standard carbon fibers like T300 and T1000.

Using thin wound or sputtered gold wires as motor coils reduces eddy current losses to a tolerable amount. Studies have shown that even small motors that use Halbach arrays and air spools reach efficiencies of more than 90%. This allows the use of highly efficient, permanent magnet excited motors with very low standby-losses.

Outlook

If techniques are developed to produce CNTs in a cost efficient manner and in larger filaments, they will increase energy densities by a factor of 10 compared to current

CFRP FESSs. High life expectations and fast charge and discharge times make FESSs particularly interesting for energy storage devices in the future, like in cases of power backup, fast acting energy harvesting applications and mobile applications for wireless sensor actor networks and overcome their relatively expensive manufacturing.

References

- Abdi, B., J. Milimonfared, and J. S. Moghani. 2010. "Simplified Design of Slotless Halbach Machine for Micro-Satellite Electro-Mechanical Batteries." Power Electronics, Machines and Drives (PEMD 2010) 5th International Conference, April 19–21, 1–5.
- Bleuler, H., and J. Sandtner. 2005. *Passive Magnetic Bearing for Flywheels*. Berlin: Springer, Solid mechanics and its applications.
- Faulhaber. 2013. "DC-Micromotor Series 0816...SR."
- Feldhusen, K.-H. G. 2001. "DUBBEL-Taschenbuch für den Maschinenbau."
- Ghoniem, A. F. 2011. "Needs, Resources and Climate Change: Clean and Efficient Conversion Technologies." *Progress in Energy and Combustion Science* 37:15–51.
- Hu, Y.-S. 2007. Patent No. WO/2007/137794. München.
- Kolk, M. 1997. *Ein Schwungrad-Energiespeicher Mit Permanentmagnetischer Lagerung*. Jülich: Forschungszentrum Jülich.
- Kratt, K. 2010. *Microcoils Manufactured with a Wire Bonder*. Freiburg: Albert-Ludwigs-Universität Freiburg.
- LaunchPoint Technologies Inc. 2009. LaunchPoint Technologies Inc. (LAUNCHPOINT) Retrieved from <http://www.launchpnt.com/portfolio/transportation/halbach-electric-motor/>
- Merritt, B. T., and R. F. Post. 1994. "Halbach Array Motor/Generators – A Novel Generalized Electric Machine." Department of Energy by Lawrence Livermore National Laboratory, USA.
- Sandtner, J., and H. Bleuler. 2004. "Electrodynamic Passive Magnetic Bearing with Planar Halbach Arrays." Ninth International Symposium on Magnetic Bearings, August 3–6.
- Tarrant, C. D. 1993. Patent No. WO1994006193 A1. GB.
- Torayca. n.d. T1000 Data Sheet.
- Torayca. n.d. T300 Data Sheet.
- Wrede, C. 1998. *Schwungmassen-Energiespeicher Mit Integrierten Funktionselementen*. Braunschweig: RTWH Aachen.
- Yi, J., and Lee, K. W. 2007. "Micro Flywheel Energy Storage System with Axial Flux Machine." IEEE, September 4–7, 1–6.
- Yoo, S. Y., and H. C. Lee. 2008. "Optimal Design of Micro Flywheel Energy Storage System." International Conference on Control, Automation and Systems, In COEX, October 14–1.
- Yu, M.-F. 2000. "Tensile Loading of Ropes of Single Wall Carbon Nanotubes and Their Mechanical Properties." *The American Physical Society* 84:5552–55.